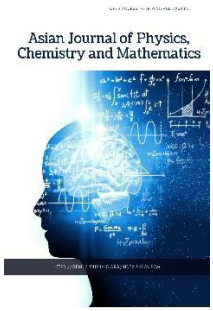

Structural, Magnetic Properties of $Ni_{x-1}Zn_xFe_2O_4$Nanocrystals by co-precipitation method.

Omar A. Ahmed[1], The General Directorate for Education in Diyala, Diyala, Iraq

Hamed A. Younis[2] The General Directorate for Education in Diyala, Diyala, Iraq

Wissam A. Hussian[3] The General Directorate for Education in Diyala, Diyala, Iraq

Ahmed M. Shano[4] Bilad Alrafidain University College, Department of radiological techniques, Diyala, Iraq

ABSTRACT

The compound $Ni_{x-1}Zn_xFe_2O_4$ ($0 \le x \le 1$) was prepared by co-precipitation method. The structural and morphological aspects were evaluated by X-ray powder diffraction (XRD), scanning electron microscopy (SEM), infrared Spectroscopy (FTIR), The magnetic properties were evaluated using vibration Sample magnetometer (VSM). The replacement of zinc in the $Ni_{x-1}Zn_xFe_2O_4$ nanocrystals increased the lattice parameter of the ferrite nanoparticles monotonically from 8.388 to 8.422 Å and decreased the size of the nanocrystals from 16.56 to 12.95 nm. FTIR spectroscopy showed that replacement with Zn up to x = 0.5 in $Ni_{x-1}Zn_xFe_2O_4$ nanocrystals led to the migration of iron ions from tetrahedral to octahedral sites, which led to an improvement in the value of the saturation magnetization which reached to 47.6 emu / g. At the same time, the coercivity decreased from 45.2 O_e to 10.6 O_e due to the increment in zinc content except for the sample x = 0.5.

Keywords: Co-precipitation, Ni–Zn magnetic nanoparticles, Spinel structure, SEM.

1.Introduction

The multifunctionality in the use of nanomaterials results from their distinctive physical and chemical properties compared to other types of materials. The availability of specific properties of spinel ferrite MFe_2O_3 (M = divalent metal ion) makes it extremely important in several fields of applications for example in magnetic storage devices, Ferro fluids , catalysts, rod antennas, electrodes in energy storage devices, microwave devices [1-4] , spintronic devices [5], magnetically recoverable catalysts [6-7], Nano-carriers for drug delivery [9,10]. The structural and magnetic properties of this type depend mainly on the positive distribution between positions (A) and (B) in the face-centered cubic spinel structure [11], stoichiometry, and the method of synthesis [12].

NiFe2O4 is a soft magnetic material that has many applications in various technological fields due to its magnetic properties, low eddy current losses and catalytic behavior. The distribution and type of cations in octahedral and tetrahedral positions control the magnetic properties of nickel ferrite. In addition to the preparation methods that determine the structural properties of the resulting materials through particle size [13]. There are a variety of ferrite spinel that have attracted a great deal of interest. The Ni-Zn mixed type showed outstanding properties in magnetism, most versatile to use, and good chemical stability [14,15].

2.Synthesis of Ferrite Nanoparticles

Chemical co-precipitation method had been used to prepare the magnetic nanoparticles $Ni_{x-1}Zn_xFe_2O_4$ where (x= 0 to 0.5). Stoichiometric amount of the reactants of $FeCl_3$, $NiCl_2.6H_2O$ and $ZnCl_2$ were dissolved in separate beakers contain 100ml with de-ionized water. The dissolved salts were mixed in another beaker with continuously stirring getting aqueous solution. Furthermore 5g of NaOH was dissolved individually in 100ml of de-mineralized water. The base solution is regularly drips into metal salt solution at (27-30°C) with continuously stirring. The pH of the solution is adjusted to 12.5 in order to ensure the precipitation of all metal ions. The solution color had changed to black.

Then the precipitate solution was heated at 90°C for an hour with constant stirring and left to cool at room temperature. The precipitates settle down in the beaker bottom. The precipitates are separated by filter paper and washed for several times with de-mineralized water until neutralize the out products water. Small amount of the obtained product was dried at 50°C to examine phase composition by XRD analysis, and studying the morphology, and size through using FESEM images. The wet product had re-dispersed in the NaOH solution (pH=13) by stirring the mixture for 1 hour, this process made it ready to the upcoming step. In order to avoid the coalescence of the adjacent particles mostly happening in the sintering process at high temperature, where the particles became in contact with each other. So the next step of the preparation method is the heat treatment to be carried out by hydrothermal method. The colloidal solution transferred to the Teflon covered autoclave reactor of 200 mL capacity. The Autoclave is sealed and placed in furnace at 220°C for 3 h, then autoclave has been allowed to cool down at room temperature naturally. One more time the colloidal solution is filtered and frequently washed with de-mineralized water until neutralized the discharged solution that is finally dried at 50°C .

3.Results and discussion

3.1.XRD Analyses

Figure 1. illustrates the XRD pattern of samples $Ni_{x-1}Zn_xFe_2O_4$ (x=0-0.5) prepared by co-precipitation method. it was noticed that the formation of single phase $Ni_{x-1}Zn_xFe_2O_4$ was consistent with the powder diffraction file of (JCPDS Card No. 22-1086 with a = 8.381 Å for $NiFe_2O_4$ and JCPDS Card No. 89-1012, with a=8.433Å for $ZnFe_2O_4$,respectively). The analysis Diffraction pattern using (2 2 0), (3 1 1), (4 0 0), (4 2 2), (5 1 1), (4 4 0), (6 2 0), and (5 3 3) reversal levels confirm the formation of the cubic spinel structure. The lattice constant in the crystal structure can be calculated by using equation (1) where (d) is the distance between two adjacent planes in the crystal and (hkl) Miller's indices.

$$\frac{1}{d^2} = \frac{h^2+k^2+l^2}{a^2} \quad \text{.... (1)}$$

The crystal size of the samples was determined, according to Eq. (2). Which shows the mean crystal size and standard deviation from XRD with the change in the values of x. Where (D) represents the average crystal size, (λ) the wavelength of the X-ray used = 1.5406 Å, (K) a constant (0.94), β Full width at Half Maximum (FWHM) measured in radial units , (θ) the Bragg angle, and (ε) strain . [16]

$$\beta \cos\theta = \frac{k\lambda}{D} + 4\varepsilon \sin\theta \quad \text{..... (2)}$$

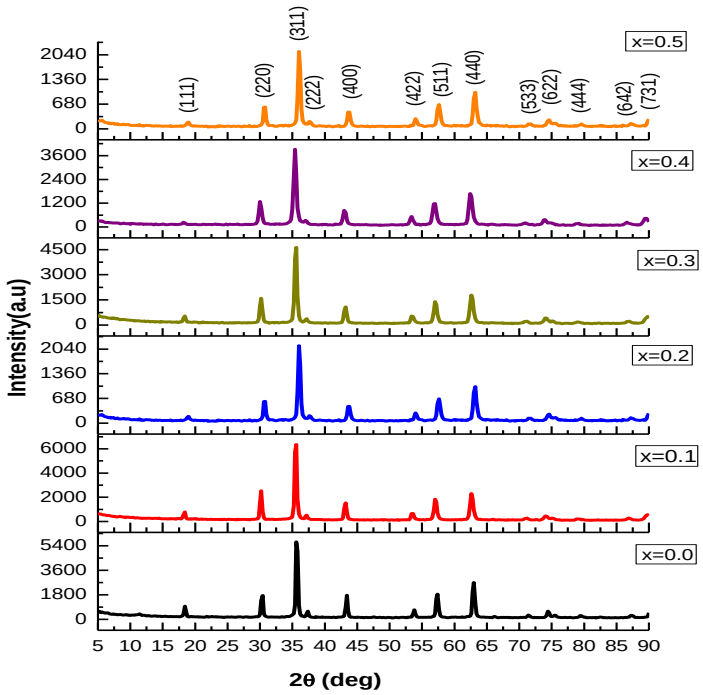

Fig. 1 XRD spectra of the $Ni_{x-1}Zn_xFe_2O_4$ nanoparticles synthesized by co-precipitation method.

Table1 shows Plotting the lattice parameter as a function of x amount of zinc substitution $Ni_{x-1}Zn_xFe_2O_4$ derived from the XRD spectra. It can be seen that in this case, the lattice parameter increases linearly with increasing x, since zinc cations with ionic radius (0.82 Å) replace Ni cations with ionic radius (0.78 Å) and thus the crystal expands slightly and this is in agreement with Wiegard's law. The increment of the lattice constant with the increasing of zinc concentration is within the range of the lattice constants for $NiFe_2O_4$ and $ZnFe_2O_4$ [14,17].

Table1 X-ray analysis of $Ni_{x-1}Zn_xFe_2O_4$ ($0 \le x \le 0.5$) samples.

Composition	Zn content (*x*)	Lattice parameter *a* (Å)	Strain ε ($\times 10^{-3}$)	Crystallite size *D* (nm)
$NiFe_2O_4$	0	8.388	0.000226	16.56
$Ni_{0.9}Zn_{0.1}Fe_2O_4$	0.1	8.392	0.000314	14.03
$Ni_{0.8}Zn_{0.2}Fe_2O_4$	0.2	8.402	0.000525	14.77
$Ni_{0.7}Zn_{0.3}Fe_2O_4$	0.3	8.411	0.000575	13.68
$Ni_{0.6}Zn_{0.4}Fe_2O_4$	0.4	8.417	0.000823	13.91
$Ni_{0.5}Zn_{0.5}Fe_2O_4$	0.5	8.422	0.00122	12.95

The strain is lowest in the sample containing a higher concentration of nickel and increases with increasing zinc concentration. Doping of Zn^{2+} ions at the Ni^{2+} site increases the lattice strain because of the large ionic diameter of the zinc ions [18].

3.2.SEM analysis

Fig. 2 SEM images of the ferrite structure $Ni_{x-1}Zn_xFe_2O_4$. show that the grain size of all samples ranged from 52nm to 78nm. An increase in zinc substitution leads to an increase in the grain size. We note that the granules are formed regularly and the agglomeration increases with the increase in the zinc content.

Fig. 2 SEM image of the synthesized $Ni_{x-1}Zn_xFe_2O_4$ ($0 \le x \le 0.5$) nanocrystals.

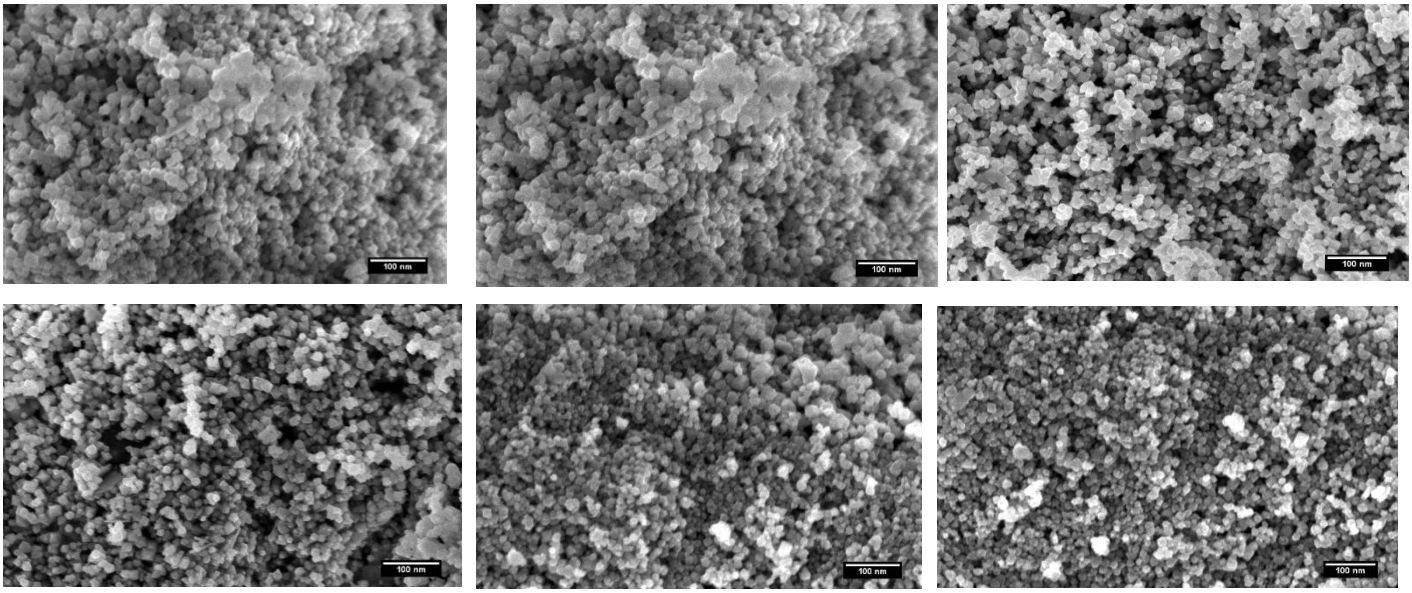

3.3. FTIR analysis

Fig.3 shows the FT-IR spectra of the compound $Ni_{x-1}Zn_xFe_2O_4$ and confirms the formation of the spinel structure, which is consistent with X-ray analysis. Two of the main absorbances are within the range (590-370 cm^{-1}) where connections are observed in the range (587-541 cm^{-1}) and (437-374 cm^{-1}). These bonds are due to the vibration of both tetrahedral and octahedral metals with oxygen (M-O) in the lattice, respectively [19]. We note the change in the frequency of the bonds with the change in the content of zinc ions.

From the table 2, we find that the values of υ_1 decrease while υ_2 increases with the increase in the content of zinc ions due to the presence of added zinc ions with the largest ionic radius and the largest atomic weight at the tetrahedral sites, which makes

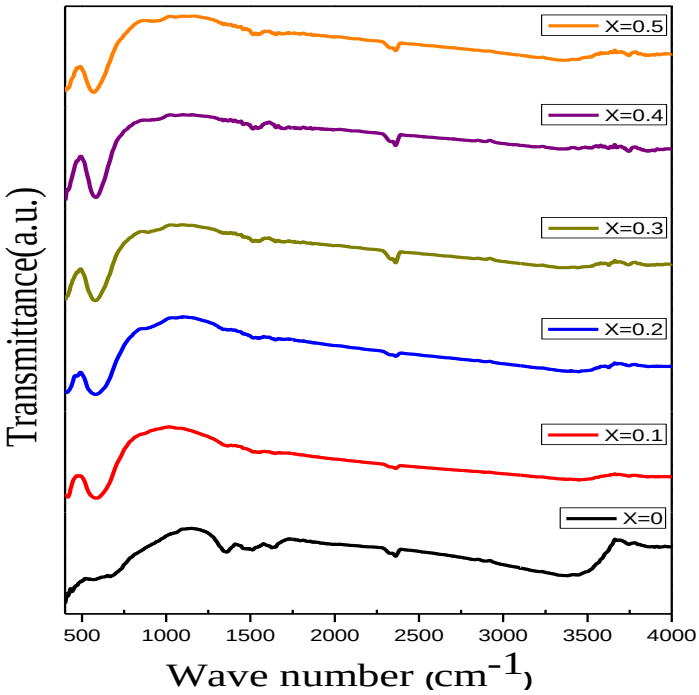

Fig. 3 FT-IR spectra of $Ni_{x-1}Zn_xFe_2O_4$ (0≤x≤0.5) nanoparticles.

The iron ions move to the octahedral sites, leading to the reduction of tetrahedral vibration frequency. For the same reason, the migration of iron ions to the octahedral sites leads to an increase in the octahedral vibration frequency [20,21].

Table 2 FT-IR absorption band frequencies of Ni1−*x*Zn*x*Fe2O4 (0≤x≤0.5) nanocrystals.

Composition	Zn content *(x)*	FT-IR frequency bands *(*cm−1*)*	
		A-site (tet) *υ*1	B-site (oct) *υ*2
$NiFe_2O_4$	0	587.93	374.19
$Ni_{0.9}Zn_{0.1}Fe_2O_4$	0.1	563.21	387.69
$Ni_{0.8}Zn_{0.2}Fe_2O_4$	0.2	559.35	399.26
$Ni_{0.7}Zn_{0.3}Fe_2O_4$	0.3	551.64	416.41
$Ni_{0.6}Zn_{0.4}Fe_2O_4$	0.4	549.71	432.48
$Ni_{0.5}Zn_{0.5}Fe_2O_4$	0.5	541.97	437.42

3.3.VSM analysis

The magnetic properties of the compound were examined using a magnetometer (VSM) at room temperature. The figure shows (M-H) curves for compounds $Ni_{x-1}Zn_xFe_2O_4$ and the values of saturation magnetization, coercion and residual magnetization extracted from (M-H) curves are listed in the table (3).

Table .2 Magnetization measurements on $Ni_{x-1}Zn_xFe_2O_4$ (0≤x≤0.5) samples.

Composition	Zn content *(x)*	Saturation Magnetization (Ms) emu/gm	Coercivity (Hc) Oe
$NiFe_2O_4$	0	1.6	45.2
$Ni_{0.9}Zn_{0.1}Fe_2O_4$	0.1	2.7	39.4
$Ni_{0.8}Zn_{0.2}Fe_2O_4$	0.2	8.3	35.5
$Ni_{0.7}Zn_{0.3}Fe_2O_4$	0.3	9.2	14.3
$Ni_{0.6}Zn_{0.4}Fe_2O_4$	0.4	47.6	10.6
$Ni_{0.5}Zn_{0.5}Fe_2O_4$	0.5	18.4	248.4

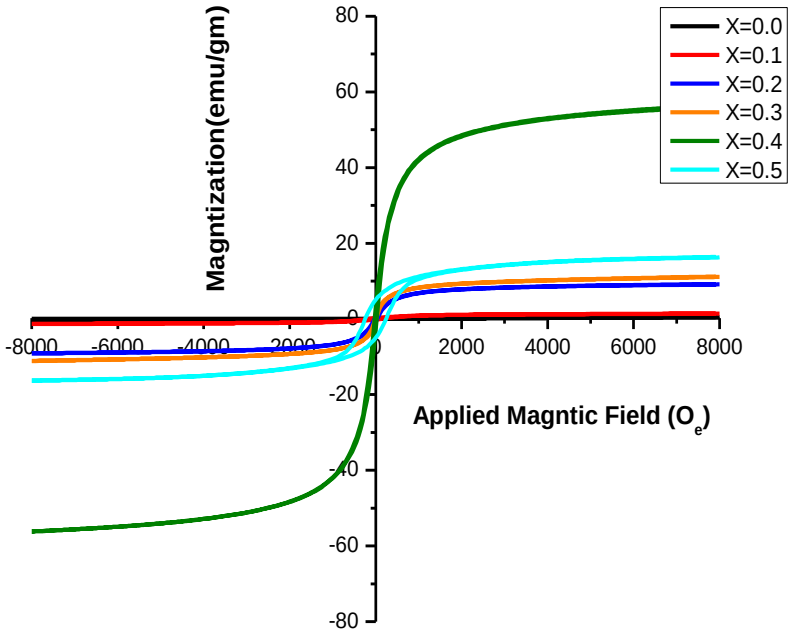

Fig. 4 Hysteresis curves of $Ni_{x-1}Zn_xFe_2O_4$ ($0 \le x \le 0.5$) nanocrystals at room temperature.

The saturation magnetization value of $Ni_{x-1}Zn_xFe_2O_4$ in the (M - H) curve is increasing with the increase of zinc ions content and this is consistent with (FTIR) analysis. The increase in saturation magnetization is described on the basis of the Neale model for subnetworks. The magnetic behavior depends on the occupancy of tetrahedral and octahedral sites in ferromagnetic (Fe^{3+}, Ni^{2+}) and non-magnetic (Zn^{2+}) ions.

Occupancy of the zinc ions replaced by nickel ions on tetrahedral sites bring about the relocation of iron ions to octahedral sites due to their bias polarization effect. The distribution of the cations depends on their electronic arrangement as well. The decrease in saturation magnetization at (X = 0.5) is due to the ratio of zinc ions to the number of iron ions in the tetrahedral sites, which leads to a weak (A-B) reaction and a change in the (B-B) reaction from a ferromagnetic to an antiferromagnetic state [21,22,23].

The coactivity of the compound declines with the increment of the zinc ions concentration except sample (x= 0.5) due to the decline in magneto-crystalline anisotropy Because the anisotropy of zinc is less than that of nickel [24]. It is noted that the coercion increases for x = 0.5. This indicates that in the Ni-Zn nano-ferrites, coercivity due to anisotropy is the main contributor. In the case of Ni-Zn nanocrystal line ferrites, the presence of a facile magnetic axis is unknown. Participation of the disparity of form is dominant in the coercion mechanism. It is also known that factors such as the grain size, the size of the domains, and the nature of the domains have a strong influence in finding the coercivity of a substance [25].

4. Conclusion

It was experimentally studied how a compound $Ni_{x-1}Zn_xFe_2O_4$ affected by zinc doping. These samples were prepared by co-precipitation and various structural and magnetic measurements were made on them. The crystalline size of the as-synthesized nanocrystals was calculated using Williamson-Hall formula within the range of 1.4-19.6 nm. VSM showed that both magnetic properties are due to competition from ferromagnetic Ni^{2+}, Fe^{3+} and non-magnetic Zn^{2+} ions, and to tetrahedral and octahedral occupations sites. The FTIR Spectroscopy showed that the substitution with Zn in $Ni_{x-1}Zn_xFe_2O_4$ nanocrystals cause iron migration from

tetrahedral sites to octahedral sites. Furthermore, it has been shown that, as in the bulk case, Zn^{2+} cations are preferred to replace Fe^{3+} ions at the tetrahedral sites.

VSM measurements, showed an increase in saturation magnetization (Ms) with Zn/Ni content and a decrease at (H_C). This is due to the increased content of Fe^{3+} ions at the octahedral sites. This increase in saturation magnetization is highest in the case of $Ni_{0.6}Zn_{0.4}Fe_2O_4$ nanoparticles. And all samples exhibited an ultra-magnetic behavior.

References

1. J. Mantilla, L.León Félix, M.A. Rodriguez, F.H. Aragon, P.C. Morais, J.A.H. Coaquira,E. Kuzmann, A.C. de Oliveira, I. Gonzalez, W.A.A. Macedo, V.K. Garg, Washing effect on the structural and magnetic properties of $NiFe_2O_4$ nanoparticles synthesized by chemical sol-gel method, Materials Chemistry and Physics,213(2018) 295-304.
2. D.K. Dinkar, B. Das, R. Gopalan, B.S. Dehiya, Effects of surfactant on the structural and magnetic properties of hydrothermally synthesized $NiFe_2O_4$ nanoparticles, MaterialsChemistry and Physics,218 (2018) 70-76.
3. K. Kombaiah, J.Judith Vijaya, L.John Kennedy, K. Kaviyarasu, Catalytic studies of $NiFe_2O_4$ nanoparticles prepared by conventional and microwave combustion method, Materials Chemistry and Physics,221 (2019) 11-28.
4. A.C.F.M.Costaa,,V.J.Silvaa,D.R.Cornejob, M.R.Morellic,R.H.G.A. Kiminamic, L.Gamaa, Magnetic and structural properties of $NiFe_2O_4$ ferrite nanopowder doped with Zn^{2+},Journal of Magnetism and Magnetic Materials 320 (2008) e370–e372.
5. W.E. Mahmoud, Observation of room temperature ferromagnetism with giant magnetic moment based on $Zn_{1-x}Cr_xO$ thin films grown on Si (111) substrate via 1,2-dihydroxyethane modified sol-gel dip-coating technique, Mater. Lett. 177 (2016) 42-45.
6. R. Easterday, O. Sanchez-Felix, Y. Losovyj, M. Pink, B.D. Stein, D.G. Morgan, M. Rakitin, V.Y. Dolud, M.G. Sulman, W.E. Mahmoud, A.A. Al-Ghamdi and L.M. Bronstein, Design of ruthenium/iron oxide nanoparticle mixtures for hydrogenation of nitrobenzene, Catal. Sci. Technol. 5 (2015) 1902-1910.
7. E.Y. Yuzik-Klimova, N.V. Kuchkina, S.A. Sorokina, D.G. Morgan, B. Boris, L.Zh. Nikoshvili, N.A. Lyubimova, V.G. Matveeva, E.M. Sulman, B.D. Stein, W.E. Mahmoud, A.A. Al-Ghamdi, A. Kostopoulou, A. Lappas, Z.B. Shifrina, L.M. Bronstein, Magnetically Recoverable Catalysts Based on Polyphenylenepyridyl Dendrons and Dendrimers, RSC Adv. 4 (2014) 23271-23280.
8. Y.A. Kabachii, A.S. Golub, S.Yu. Kochev, N.D. Lenenko, S.S. Abramchuk, M.Y. Antipin, P.M. Valetsky, B.D. Stein, W.E. Mahmoud, A.A. Al-Ghamdi, L.M. Bronstein, Multifunctional Nanohybrids by Self-Assembly of Monodisperse Iron Oxide Nanoparticles and Nanolamellar MoS2 Plates, Chem. Mater. 25 (12) (2013) 2434–2440.
9. W.E. Mahmoud, F. Al-Hazmi, F. Al-Noaiser, A.A. Al-Ghamdi, L.M. Bronstein, A facile method to syntheses monodisperse γ-Fe_2O_3 nanocubes with high magnetic anisotropy density, Superlat. Microstruct. 68 (2014) 1-5.
10. F.S. Al-Hazmi, A.A. Al-Ghamdi, G.W. Beall, L.M. Bronstein, W.E. Mahmoud, Synthesis and characterization of 4-amino-3-isoxazolidinone intercalated NiAl-LDH for nanocarrier applications, Colloid. Surface A: Physicochem. Eng. Asp. 485 (2015) 91-95.
11. F. Li, H. Wang, L. Wang, J. Wang, Magnetic properties of $ZnFe_2O_4$ nanoparticles produced by a low-temperature solid-state reaction method, J. Magn. Magn. Mat. 309 (2007) 295-299.
12. D.V. Kurmude , R.S. Barkule ,A.V. Raut ,D.R. Shengule ,K.M. Jadhav, X-Ray Diffraction and Cation Distribution

Studies in Zinc-Substituted Nickel Ferrite Nanoparticles, J Supercond Nov Magn,27(2014) 547–553.

13. F. Majid, J. Rauf, S. Ata, I. Bibi, A. Malik, S.M. Ibrahim, A. Ali, M. Iqbal,Synthesis and characterization of $NiFe_2O_4$ ferrite: Sol–gel and hydrothermal synthesis routes effect onstructural, magnetic and dielectric properties, Materials Chemistry and Physics,258(2021) 123888.
14. B. Rabi1, A. Essoumhi1, M. Sajieddine , E. K. Hlil , A. Razouk , R. Moubah, H. Lassri, Study of the Magnetocaloric Effect in $Ni_{1-x}Zn_xFe_2O_4$ Spinel, Journal of Superconductivity and Novel Magnetism,33(2020)2527–2534.
15. A. Bajorek, C. Berger, M. Dulski, P. Łopadczak, M. Zubko, K. Prusik, M.Wojtyniak, A. Chrobak, F. Grasset, N. Randrianantoandro, Microstructural and magnetic characterization of $Ni_{0.5}Zn_{0.5}Fe_2O_4$ ferrite nanoparticles, Journal of Physics and Chemistry of Solids,129 (2019)1-21.
16. Tagreed M. Al-Saadi, Omar A. Ahmed, Imad H. Khaleel, T.A.AL- Dhahir, The effect of the Doping with Cobalt Transition Metal on the Dielectric and Structural Properties of $Fe_{0.5}Co_xMg_{0.95-x}O$ Nanoparticles Synthesized by Sol-Gel Assisted Auto Combustion, Journal of Physics: Conference Series, 1879 (2021) 032117.
17. S.S. Deshmukh, A.V. Humbe, A. Kumar, R.G. Dorik, K.M. Jadhav, Ureaassisted synthesis of $Ni_{1-x}Zn_xFe_2O_4$ ($0 \le x \le 0.8$): Magnetic and Mössbauer investigations, Journal of Alloys and Compounds,704(2017) 227-236.
18. P.Surendran, A.Lakshmanan, S. Sakthy Priya, K. Balakrishnan, P. Rameshkumar, Tejaswi Ashok Hegde, G. Vinitha, G. Ramalingam, A. Antony Raj, Investigations on solid-state parameters of third-order nonlinear optical $Ni_{1-x}Zn_xFe_2O_4$ nanoparticles synthesized by microwave-assisted combustion method Applied Physics A,126(2020)257.
19. M. Salavati-Niasari , F. Davar , T. Mahmoudi , A simple route to synthesize nanocrystalline nickel ferrite ($NiFe_2O_4$) in the presence of octanoic acid as a surfactant ,Polyhedron ,28 (2009) 1455–1458.
20. F. Shahbaz Tehrani,V. Daadmehr, A.T. Rezakhani,R. Hosseini Akbarnejad,S. Gholipour, Structural, Magnetic, and Optical Properties of Zinc- and Copper-Substituted Nickel Ferrite Nanocrystals Journal of Superconductivity and Novel Magnetism,25(2012) 2443–2455.
21. P.P. Hankare, R.P. Patil, A.V. Jadhav, R.S. Pandav, K.M. Garadkar, R. Sasikala, A.K. Tripathi, Synthesis and characterization of nanocrystalline Ti- substituted Zn ferrite, J. Alloys Compd. 509 (2011) 2160-2163.
22. M. Sertkol, Y. Köseoglu , A. Baykal, H. Kavas , A. Bozkurt, M.S. Toprak , Microwave synthesis and characterization of Zn-doped nickel ferrite nanoparticles, Journal of Alloys and Compounds, 486 (2009) 325–329.
23. Ahmed A. Al-Ghamdi, Farag. S. Al-Hazmi, Leena S.Memesh, F.S. Shokr, Lyudmila M. Bronstein, Effect of mechanochemical synthesis on the structure, magnetic and optical behavior of $Ni_{1-x}Zn_xFe_2O_4$ spinel ferrites, Journal of Ceramics International,43(2017) 6192-6200.
24. S. P. Iglesias, A. Arias-Durán, J. M. Yañez-Limón, R. Ramirez-Bon, A. Hurtado-Macias, O. Arnache,M. E. Gómez,W. Lopera, G. Zambrano, Effect of Zn Concentration on the Structure, Morphology, and Magnetic Behavior of $Ni_{1-x}Zn_xFe_2O_4$Ferrofluid, Journal of Superconductivity and Novel Magnetism,32(2019) 2199–2208.
25. P.S. Hedaooa, D.S. Badwaika, S.M. Suryawanshia, K.G. Rewatkar, Structural and Magnetic Studies of Zn Doped Nickel Nanoferrites Synthesize by Sol-gel Auto Combustion Method, Materials Today: Proceedings,15 (2019) 416–423.